CEST MRI Provides Amides/amines Surrogate Biomarkers for Treatment-naïve Glioma Sub-typing

Laura Mancini (lmancini@nhs.net)
University College London Hospitals NHS Foundation Trust https://orcid.org/0000-0002-4596-3551
Stefano Casagranda
: Olea Medical
Guillaume Gautier
: Olea Medical
Philippe Peter
: Olea Medical
Bruno Lopez
: Olea Medical
Lewis Thorne
UCLH NHNN: National Hospital for Neurology and Neurosurgery
Andrew McEvoy
UCLH NHNN: National Hospital for Neurology and Neurosurgery
Anna Miserocchi
UCLH NHNN: National Hospital for Neurology and Neurosurgery
George Samandouras
UCLH NHNN: National Hospital for Neurology and Neurosurgery
Neil Kitchen
UCLH NHNN: National Hospital for Neurology and Neurosurgery
Sebastian Brandner
UCLH NHNN: National Hospital for Neurology and Neurosurgery
Enrico De Vita
UCLH NHNN: National Hospital for Neurology and Neurosurgery
Francisco Torrealdea
UCLH: University College London Hospitals NHS Foundation Trust
Marilena Rega
UCLH: University College London Hospitals NHS Foundation Trust
Benjamin Schmitt
Siemens Healthineers: Siemens Healthcare GmbH
Patrick Liebig
Siemens Healthineers: Siemens Healthcare GmbH
Eser Sanverdi

UCLH NHNN: National Hospital for Neurology and Neurosurgery

Xavier Golay

UCL Institute of Neurology: UCL Queen Square Institute of Neurology

Sotirios Bisdas

UCLH NHNN: National Hospital for Neurology and Neurosurgery

Research Article

Keywords: isocitrate dehydrogenase, 1p/19q codeletion, oligodendroglioma, chemical exchange saturation transfer, glioma risk stratification

Posted Date: October 18th, 2021

DOI: https://doi.org/10.21203/rs.3.rs-887227/v1

Version of Record: A version of this preprint was published at European Journal of Nuclear Medicine and Molecular Imaging on January 14th, 2022. See the published version at https://doi.org/10.1007/s00259-022-05676-1.

Abstract

Purpose

Accurate gliomas classification affects patient management and is challenging on non- or low-enhancing gliomas. This study investigated the clinical value of different Chemical Exchange Saturation Transfer (CEST) metrics for glioma classification and assessed the diagnostic effect of the presence of abundant fluid in gliomas subpopulations.

Methods

Forty-five treatment-naïve glioma patients with known isocitrate dehydrogenase (IDH) mutation and 1p/19q codeletion status received CEST MRI at 3T. Magnetisation transfer ratio asymmetry and CEST metrics (amides: offset range 3-4ppm, amines: 1.5-2.5ppm, amides/amines ratio) were calculated with two models: ‘asymmetry-based’ (AB) and ‘fluid-suppressed’ (FS). Presence of T2/FLAIR mismatch was noted.

Results

IDH-wildtype had higher amides/amines ratio than IDH-mutant_1p/19q^{codel} ($p<0.022$). Amides/amines ratio and amines levels differentiated IDH-wildtype from IDH-mutant ($p<0.0045$) and from IDH-mutant_1p/19q^{ret} ($p<0.021$). IDH-mutant_1p/19q^{ret} had higher amides and amines than IDH-mutant_1p/19q^{codel} ($p<0.035$). IDH-mutant_1p/19q^{ret} with AB/FS mismatch had higher amines than IDH-mutant_1p/19q^{ret} without AB/FS mismatch ($p<0.016$). In IDH-mutant_1p/19q^{ret}, the presence of AB/FS mismatch was closely related to the presence of T2/FLAIR mismatch ($p=0.014$).

Conclusions

CEST-derived biomarkers for amides, amines and their ratio can help with histomolecular staging in gliomas without intense contrast enhancement. T2/FLAIR mismatch is reflected in the presence of AB/FS CEST mismatch. The AB/FS CEST mismatch identifies glioma sub-groups that may have prognostic and clinical relevance.

Introduction

The discovery of mutations in the IDH1 and IDH2 genes in astrocytic and oligodendroglial tumours has led to a biomarker-driven classification, forming an integrated diagnosis composed of the histological appearance and the molecular profile [1].

Currently, two types of IDH-mutant gliomas are identified. The IDH-mutant astrocytoma is defined by an additional mutation of ATRX and p53. A loss in the tumour suppressor locus CDKN2A/B is an important additional prognostic marker, typically found in IDH-mutant glioblastomas. The IDH-mutant oligodendroglioma is defined by an absent ATRX mutation, and a codeletion of chromosomal arms 1p

and 19q. IDH-mutant oligodendrogliomas consistently carry a TERT promoter mutation. The IDH-wildtype gliomas comprise a wide range of tumours, including but by far not limited to, the IDH-wildtype glioblastoma. The IDH-wildtype glioblastoma is molecularly characterised by chromosome 7 gain, chromosome 10 loss, frequent EGFR amplification and TERT promoter mutation. However, there is a wide range of other IDH-wildtype gliomas of low and high grades, with other defining mutations, such as BRAF, histone H3 K27M, H3 G34R.

Several advanced MRI exploiting different tissue compositions and properties have been shown to add diagnostic and prognostic value to the conventional gadolinium-enhanced MRI protocols, which cannot reliably sample the genetic makeup of the tumours. Examples are diffusion-weighted imaging (DWI) [2-6], perfusion-weighted imaging [7-10], magnetic resonance spectroscopy (MRS) [11, 12] and, recently, chemical exchange saturation transfer (CEST). CEST MRI is based on proton-exchange properties and allows imaging of low concentration metabolites (concentrations in vivo down to mM range) with enhanced sensitivity indirectly through the water signal [13, 14]. The CEST MRI signal detectable from amide protons (–NH groups resonating at 3.5ppm downfield from the water peak) and of the amine protons ($–NH_2$ groups, at 2ppm), present in endogenous proteins and peptides, have been shown in small patient cohorts and feasibility studies to differentiate: low-grade gliomas from high-grade gliomas [15-17] with better diagnostic performance than diffusion- and perfusion-weighted imaging [18-20]; tissue heterogeneities in high-grade gliomas [21]; tumour progression from radiation necrosis [22, 23]; IDH-wildtype from IDH-mutant glioma [24]; and IDH-mutant with 1p/19q codeletion from 1p/19q-intact IDH-mutant glioma [24, 25]. CEST-derived metrics have also been shown to correlate with patient overall survival and progression-free survival [26-28].

The current evidence for the clinical utility of CEST metrics has inherent study design and methodological weaknesses. The former includes mainly the small number of patients; the unbalanced cohort composition with diagnostically straightforward, by means of conventional MRI, high-grade gliomas; and the use of the outdated WHO 2007 classification for glioma grading in the prevailing number of studies. Methodological issues are related to the investigation only of the 3.5ppm amides frequency and negligence of the T2/FLAIR mismatch effect on the CEST maps, which carries significant diagnostic implications as CEST is sensitive to fluid signal [29]. Studies in rats and phantoms have suggested that the CEST contribution at 2ppm is sensitive to proteins, amino acid and pH concentration changes, and may serve as a sensitive neuroimaging biomarker for many diseases [30], whilst a study in vitro and on mice has suggested the amides/amines ratio to be sensitive to the tissue acidity in stroke [31].

The current study sought to address the knowledge gap on the clinical value of CEST imaging to predict the histo-molecular glioma type by prospectively investigating the whole range of frequency offsets either side of the water peak from 0 to 4 ppm in a single-centre setting, large patient cohort presenting mainly with the diagnostically challenging primary gliomas with absent or weak enhancement. For the first time, we sought to evaluate the diagnostic value of tumour amides/amines ratio, which might be a promising surrogate biomarker for gliomas sub-typing. We also aimed to assess the diagnostic sensitivity and specificity of two different CEST models (‘asymmetry-based’ and ‘fluid-suppressed’) to address any

diagnostic compromise caused by the presence of abundant fluid in gliomas subpopulations, i.e. those with T2/FLAIR mismatch.

Materials And Methods

Patients

Treatment-naïve patients, older than 18 years of age, with presumed glioma suitable for surgical lesion sampling or resection were selected during the weekly-held multidisciplinary tumour board meeting by unanimous agreement among the clinical and neuroradiology board members. Exclusion criteria included usual contraindications to MRI, pregnancy and incapacity to provide informed consent. Eighty-two patients have been so far successfully recruited for the study. For the objectives of this publication, an interim study analysis of 68 patients with conventional indeterminate MRI findings for glioma staging was conducted (Fig 1). After the MRI, 48 patients underwent surgical resection and four had a biopsy. Of these, 49 patients had histologically confirmed gliomas with grade II or higher and two patients had acute inflammation and multifocal cortical ischaemia, respectively. Data from four patients were discarded due to presence of artefacts. The MRIs of nine out of 45 patients showed post-contrast enhancement, of which seven were described as faint enhancement and two as moderate enhancement. Finally, 45 patients (19 male), who had undergone surgery/biopsy a median (range) of 1.8 (0.1–30.7) months after MRI, were included in the analysis. The clinical characteristics of the patient population are summarised in Fig 1 and detailed in Supplementary Table 1.

MRI Data Acquisition

Imaging data were acquired on a 3T whole-body MRI system (MAGNETOM Prisma; Siemens Healthcare, Erlangen, Germany) with a 64-channel Head/Neck coil. Structural T_1-weighted (T_1w), T_2w, fluid attenuated inversion recovery (FLAIR) and gadolinium-enhanced T_1w (Gd-T_1w) images were acquired with sagittal 3D Sampling Perfection with Application optimized Contrasts using different flip angle Evolution (SPACE) images, with an isotropic resolution of, respectively, 0.9x0.9x0.9mm^3, 1.1x1.1x1.1mm^3, 1.0x1.0x1.0mm^3, and 0.9x0.9x0.9mm^3. The axial single-slice prototype 2D CEST sequence was located at the largest tumour cross-section. Three acquisitions with different saturation pulse intensities were performed. A flip angle map was also acquired, to compute a relative B1 map [32]. Detailed description of the conventional MRI protocol and the CEST acquisition is provided in the Supplementary Material.

Regions of interest (ROIs)

Regions of interest (ROIs) were manually drawn by two senior neuroradiologists (12 and 8 years of experience in neuro-oncology imaging) in consensus using ITK-SNAP version 3.6 (www.itksnap.org) [33] loading first the CEST to identify the appropriate slice position and then the co-

registered FLAIR, T2w, T1w and Gd-T1w images. Areas identified were: (1) solid tumour excluding cyst and necrotic areas, (2) cyst, and (3) normal appearing white matter (NAWM) contralateral to the tumour.

CEST post-processing

CEST acquisitions were processed using prototype version software created by Olea Medical® (La Ciotat, France) for the Horizon 2020 project GLINT (number 667510). After Z-Spectra-based B_0 correction [34], the Z-Spectra at 2.0μT were B_1-corrected through an exponential fitting [32]. Magnetisation transfer ratio asymmetry (MTR_{asym}) spectra and proton transfer weighted maps with two different models and in two offset ranges were then calculated.

MTR asymmetry spectra and $DMTR_{asym}$ spectra

MTR_{asym} spectra were calculated at steps of 0.25ppm from 0ppm to 4ppm with a previously reported formula [35]. Changes in MTR_{asym} ($DMTR_{asym}$) were obtained subtracting the NAWM MTR_{asym} from the tumour one: $DMTR_{asym}(Dw) = MTR_{asym}(Dw, tumour) – MTR_{asym}(Dw, NAWM)$. Average and 25^{th} and 75^{th} percentiles of the MTR_{asym} and of the $DMTR_{asym}$ spectra from patients in the various histological groups were calculated to generate the corresponding group spectra and group range of variation.

Asymmetry-Based and Fluid-Suppressed APTw Image Processing

Non-punctual metrics [36] were adapted to generate two amides and amines proton transfer weighted maps (respectively $APT_w(D3.5)$ and $APT_w(D2)$) with improved detection of the CEST contrast for B_0- and B_1-corrected Z-Spectra at 2.0μT. APT_w maps were obtained using an asymmetry-based (AB_APT_w) model and a fluid-suppressed (FS_APT_w) model. The AB_APT_w considered only the asymmetry-average of the Z-Spectra while the FS_APT_w also attenuated the fluid signal based on the shape of Z-spectrum, as described in the Supplementary Material.

The endogenous CEST signal was explored in two offset ranges: the amines (D2, from 1.5 to 2.5ppm) and the amides ones (D3.5, from 3.0 to 4.0ppm), obtaining four maps. In total, nine normalised metrics (obtained by subtracting the average signal in the contralateral NAWM ROI from the average values in the tumour ROI) were considered: the amides, amines, and the amides/amines ratios for each of the AB, FS and AB–FS maps.

T2/FLAIR mismatch versus AB/FS mismatch in IDH-mutant gliomas

The T2 and FLAIR images were assessed in consensus by a senior neuroradiologist (14 years of experience as consultant neuroradiologist with expertise in neuro-oncology) and an MRI physicist (15 years of experience in MRI image analysis) for identification of the presence of T2/FLAIR mismatch. The T2/FLAIR mismatch was defined as the presence of >50% hyperintense signal on T_2w and relatively hypointense signal on FLAIR except for a hyperintense peripheral rim in cases of complete or near-complete mismatch [37, 38].

Cut points were calculated (method outlined in the Statistical Analysis section) for the AB–FS(D3.5) and AB–FS(D2) metrics as surrogate biomarkers to assess the presence/absence of T2/FLAIR mismatch (reference standard). The diagnostic value of AB/FS mismatch, defined as AB–FS values larger than the cut point threshold, was assessed.

Histopathology

Tumour biopsies were fixed in formalin and processed into paraffin embedded samples. Tissue sections were routinely stained with haematoxylin & eosin, and immunostained with antibodies against IDH1 R132H, ATRX, and Ki67. IDH1 R132H positive, ATRX -negative (loss of expression) were diagnosed as IDH-mutant astrocytoma, anaplastic astrocytoma, or glioblastoma, depending on the histological features. IDH1 R132H positive, ATRX -positive (retained) tumours were examined for the presence of a 1p/19q codeletion. All IDH1 R132H-negative tumours were further sequenced for the presence of a rare IDH1 or an IDH2 mutation. These tumours were also tested for TERT promoter mutation and EGFR amplification to identify the population of IDH-wildtype glioblastoma. Tumours that had no informative molecular profile, were further examined with DNA methylation arrays, followed by algorithmic classification as described in [39].

Statistical Analysis

Following a Shapiro-Wilk normality test, the asymmetry-based (AB) and fluid-suppressed (FS) CEST metrics were compared using a sign test with two-tailed p-values and significance threshold set to 0.05. A Fisher's exact test assessed the relationship between the presence/absence of AB/FS mismatch and the presence/absence of T2/FLAIR mismatch.

The Mann-Whitney U test was used to analyse the statistical differences between quantitative imaging parameters for the two IDH mutation statuses. The Kruskal Wallis test followed, when significant, by the Conover-Iman test to correct for multiple pairwise comparison (significance set to 0.05) was used to assess the statistical differences for: (i) the three glioma groups IDH-wildtype, IDH-mutant, 1p/19q^{ret} and IDH-mutant, 1p/19q^{codel}; (ii) the four tumour subgroups IDH-wildtype, IDH-mutant, 1p/19q^{ret} with (without) AB/FS mismatch, IDH-mutant, 1p/19q^{codel}. For pairs of groups with statistically significant differences after correction for multiple comparison, areas under the receiver operating characteristics (ROC) curve (AUC) and the nearest to (0,1) cut points were estimated. All statistical analyses were

performed with Stata software (StataCorp. 2017. Stata Statistical Software: Release 15. College Station, TX: StataCorp LLC).

Results

Z-Spectra, APTw maps and MTRasym and DMTRasym spectra

Representative examples of structural MRIs, CEST maps and Z-Spectra (Fig. 2) show: a cystic component present in the IDH-wildtype with reduced signal in the FS CEST maps in the amides and amines ranges (Fig. 2a, IDH-wildtype); minor differences between AB and FS maps in the solid tumour, more evident in IDH-mutant, 1p/1q^{ret} and in the amine range (Fig. 2a). Both the MTR_{asym} and the $DMTR_{asym}$ spectra showed different contributions from the amides and the amines regions between glioma subtypes over the frequency range analysed (Fig. 3).

The MTR_{asym} offset dependence is due to the presence of saturation peaks in a frequency range from –1ppm to –5ppm, mediated by the Nuclear Overhauser Enhancement (NOE). NOE is therefore entangled to the chemical exchange effect in the MTR_{asym} measure of the magnetisation transfer process. A positive MTR_{asym} reflects a predominant chemical exchange effect while a negative MTR_{asym} reflects a predominant NOE-mediated effect. In our data, the average MTR_{asym} spectrum in the NAWM over all patients was null at a frequency of ~3ppm from the water resonance (Fig. 3a), indicating a good saturation power and a small NOE contribution for frequencies above 3ppm [40, 41].

CEST metrics

Quantitatively, the derived CEST metrics with information about amides signal, amines signal and their ratios enabled the differentiation of IDH-wildtype from IDH-mutant gliomas and the identification of subgroups in the IDH-mutant gliomas (Table 1, Table 2, Fig. 4).

The amides/amines signal ratio metrics were higher in IDH-wildtype than in almost all IDH-mutant subgroups (IDH-mutant; IDH-mutant, 1p/19q^{ret}; IDH-mutant, 1p/19q^{codel} and IDH-mutant, 1p/19q^{ret} with AB/FS mismatch), but they were not significantly different between IDH-mutant subgroups. IDH-mutant subgroups were, instead, differentiated by amides, amines and AB–FS metrics.

AB versus FS metrics and AB/FS mismatch versus T2/FLAIR mismatch

The AB metrics were statistically significantly different from the FS metrics for almost all metrics and glioma subgroup, with the exception of: IDH-wildtype in the amides range; and IDH-mutant, 1p/19q^{ret}

without AB/FS mismatch in the amides range (Table 3).

A T2/FLAIR mismatch was detected only in IDH-mutant, 1p/19q^{ret} gliomas and, more specifically, in 68% (15 out of 22) of them. The difference between AB and FS metrics (AB–FS) for amides and amines (positive differences in both cases, indicating AB>FS values) allowed identifying two subgroups in IDH-mutant, 1p/19q^{ret} gliomas: those with and those without AB/FS mismatch. Cut points were calculated for the AB–FS(D3.5) metric (cut point 0.039, sensitivity 80%, specificity 71%) and AB–FS(D2) metric (cut point 0.18, sensitivity 80%, specificity 86%) as surrogate biomarkers to assess the presence/absence of T2/FLAIR mismatch, used as a reference standard.

The presence/absence of AB/FS mismatch was in agreement with the presence/absence of T2/FLAIR mismatch, as assessed by a Fisher's exact test p-value of 0.014. This indicated the presence of a significant fluid tumour component, probably micro-cysts, which are observed extracellularly in astrocytomas and intracellularly in oligodendrogliomas. Similarly, preliminary results, which will be better investigated in a future study on a larger patient cohort, showed also that the IDH-mutant, 1p/19q^{codel} gliomas could be subdivided in those with and those without AB/FS mismatch.

IDH mutation status

The amines, amides/amines signal ratio and the difference AB–FS in the amine range differentiated IDH-wildtype from IDH-mutant (Table 1, Table 2, Fig. 4). Of these metrics, the amides/amines ratio had the highest AUC (0.84 for AB and 0.81 for FS) and thresholds of 1.57 for AB (1.66 for FS) achieved 78% sensitivity and 78% specificity. In other words, IDH-wildtype had at least a 57% (66% for FS) larger signal coming from the amide component of the CEST spectrum than from the amines.

The AB–FS for amines signal was positive (AB>FS) and larger in IDH-mutant than in IDH-wildtype, suggesting the presence of a larger more "fluid" amines component in IDH-mutant gliomas (Table 3, Fig. 4).

IDH mutation and 1p/19q molecular status

When considering IDH mutation and 1p/19q molecular status, significant differences were observed in three pairwise comparisons, after correction for multiple comparisons (Table 1, Fig. 4):

1. In **IDH-wildtype vs IDH-mutant, 1p/19q^{ret}**, the highest AUC was achieved with both the amine signal (0.86 for AB and 0.81 for FS) and the amides/amines signal ratio (0.85 for AB and 0.81 for FS). The thresholds (cut points) were: 0.89 (0.76) for the AB (FS) APTw amine (lower amines in IDH-wildtype), with 77% (68%) sensitivity and 100% (89%) specificity; and 1.57 (1.59) for the AB (FS) amides/amines ratio (higher ratio in IDH-wildtype), with 78% (89%) sensitivity and 82% (72%) specificity.

2. In **IDH-wildtype** (the glioma type with the worst prognosis) **vs IDH-mutant, 1p/19q^{codel}** (the glioma type with the best prognosis): only higher amides/amines signal ratio in IDH-wildtype were observed, with both AB and FS models, with thresholds of 1.52 (1.66) for the AB (FS), 78% sensitivity for both AB and FS and specificity of 69% for AB and 77% for FS.
3. In **IDH-mutant, 1p/19q^{ret} vs IDH-mutant, 1p/19q^{codel}**, the highest AUC (0.80 for AB and 0.76 for FS) was achieved with the amines metrics (higher values in IDH-mutant, 1p/19q^{ret}), with cut points of 0.88 (0.77) for the AB (FS), sensitivity of 77% for both AB and FS and specificity of 68% for AB and 85% for FS. Other metrics that differentiated these two sub-groups were the amides and the AB–FS differences for both the amides and the amines. The AB amides metric had the highest specificity (92%), but only 55% sensitivity.

IDH mutation, 1p/19q molecular status and AB/FS mismatch

When the IDH-mutant, 1p/19q^{ret} gliomas were further subdivided in two sub-groups (with and without AB/FS mismatch), significant differences were observed in four pairwise comparisons, after correction for multiple comparisons (Table 1, Fig. 4):

1. In **IDH-wildtype vs IDH-mutant, 1p/19q^{ret} with AB/FS mismatch**, the highest AUC was achieved by the amine signal (0.97 for AB and 0.90 for FS), with thresholds of 0.89 (0.76) for the AB (FS), 93% (80%) sensitivity and 100% (89%) specificity. The amides/amines signal ratio had AUC of 0.91 (0.85) for AB (FS), thresholds of 1.39 (1.59) for the AB (FS), with 89% sensitivity and 80% specificity for both AB and FS.
2. In **IDH-wildtype** (worst prognosis) **vs IDH-mutant, 1p/19q^{codel}** (best prognosis), only higher amides/amines signal ratio in IDH-wildtype were observed with only the AB model, with AUC of 0.79, threshold of 1.53, 78% sensitivity and 69% specificity.
3. In **IDH-mutant, 1p/19q^{ret} with AB/FS mismatch vs IDH-mutant, 1p/19q^{ret} without AB/FS mismatch**, only the AB amines metric was higher in IDH-mutant, 1p/19q^{ret} with AB/FS mismatch, with AUC of 0.79, threshold of 0.82, sensitivity of 93% and specificity of 57%. The AB–FS metrics for amides and amines were different by definition (the AB/FS mismatch was defined based on the cut points on these metrics when using the T2/FLAIR mismatch as reference standard).
4. In **IDH-mutant, 1p/19q^{ret} with AB/FS mismatch vs IDH-mutant, 1p/19q^{codel}**, the highest AUC (0.90 for AB and 0.85 for FS) was achieved with the amines-related metrics, with cut points of 0.88 (0.77) for the AB (FS), sensitivity of 93% (80%) and specificity of 77% (85%). Similar AUC were also obtained with AB–FS for amines (AUC 0.90, threshold 0.042, sensitivity 93%, specificity 85%) and AB–FS for amides (AUC 0.85, threshold 0.14, sensitivity 100%, specificity 85%). The amides metrics had the highest specificity (92% for both AB and FS), but only 67% sensitivity (for both AB and FS) and AUC of 0.81 for AB and 0.79 for FS.

No metrics were statistically significant for differentiating IDH-mutant, 1p/19q^{ret} without AB/FS mismatch from IDH-mutant, 1p/19q^{codel}.

Discussion

The current study demonstrates the potential of CEST metrics using two different models and combining the signal from amides (at 3.5ppm) and amines (at 2ppm) to aid in the stratification of gliomas presenting with none or faint post-gadolinium enhancement. Results suggest that: (1) the combination of various CEST metrics may be useful biomarkers for differentiating IDH and 1p/19q status; (2) the comparison between the two models (Asymmetry Based and Fluid Suppressed) may be an objective biomarker to identify the gliomas with T2/FLAIR mismatch.

The amides/amines signal ratio was the only metric differentiating IDH-wildtype (worst prognosis) from IDH-mutant, 1p/19q^{codel} (best prognosis). The amides/amines signal ratio and levels of amine signal differentiated IDH-wildtype also from the pooled IDH-mutant and from IDH-mutant, 1p/19q^{ret}. The cut points identified for these comparisons suggested that IDH-wildtype had approximately 60% more signal originating from the amide pool than from amines groups compared to the IDH-mutant groups. IDH-mutant, 1p/19q^{ret} had higher amides and amines signal levels than IDH-mutant, 1p/19q^{codel}. The relevance of tumour acidity in differentiating gliomas with different IDH status is supported by recent studies [25, 42]. Amines and amides signal have been shown to have a complex dependency on protein, amino acids, temperature and pH concentrations, as well as on CEST saturation [30], whilst the amides/amines signal ratio has been shown to have more straighforward dependency primarily on pH when the hypothesis that amides and amines groups belong to the same molecules is valid (e.g. in ischemia) [31]. The dependency of the CEST amides/amines signal ratio on protein and amino acids concentrations cannot be asserted without additional measurements and simulations. However, the IDH-mutant, 1p/19q^{ret} without AB/FS mismatch could not be differentiated from the IDH-mutant, 1p/19q^{codel}, suggesting that the presence of T2/FLAIR mismatch, usually not assessed in the literature, is an important parameter to consider when assessing the efficiency of the CEST metrics to stratify gliomas.

A complementary imaging technique is amino acid PET (positron emission tomography), an extensively evaluated radiotracer imaging methodology that is playing an increasingly important role in the diagnosis and management of brain tumours. The advantages of amino acids PET are that radiolabelled amino acids cross the blood brain barrier and their accumulation is a function of tumour avidity for them. This differential uptake can be exploited to specifically delineate cellular mass and tumour boundaries from surrounding normal tissue also in non-enhancing gliomas [43]. A study comparing O-(2-18F-fluoroethyl)-L-tyrosine (FET) PET and APT CEST MRI in eight high-grade gliomas patients showed that FET PET and APT CEST are spatially incongruent and suggesting different biological information [44]. Even though only few studies directly compared amino acid PET and CEST in more than five patients, the complementary and additive value of these methods, as well as their incongruent findings suggest that

further investigation including also neuropathological validation could provide useful information to understand the biological information provided.

Our results also show that the asymmetry-based CEST metric is sensitive to regions with large fluid content (e.g. cystic regions), and that the fluid-suppressed (FS) metric significantly reduces the CEST signal in cysts, without affecting the signal from the normal appearing white matter, but affecting the amides and amines signals in tumour to different extent. We suggest that thresholds can be defined in the differences between the AB and FS models (AB–FS) in the amides and in the amines range, to divide the IDH-mutant, 1p/19q^{ret} gliomas in two sub-groups: with and without AB/FS mismatch (thresholds: AB–FS(D3.5) = 0.039 and AB–FS(D2) = 0.18). In IDH-mutant, 1p/19q^{ret} glioma, the presence of AB/FS mismatch was closely related to the presence of T2/FLAIR mismatch, suggesting the presence of a more fluid-like compartment but further studies are needed to explain the factors contributing to our results. As a matter of fact, presence of AB/FS mismatch and amides/amines signal ratio may be useful biomarkers for differentiating IDH-wildtype from IDH-mutant, 1p/19q^{ret} with AB/FS mismatch. However, before any meaningful clinical application may be sought, the biological and prognostic significance of the AB/FS mismatch remains to be validated in larger cohorts. Concerning IDH-mutant gliomas, combinations of amides and amines (but not amides/amines ratio) metrics may be also useful biomarkers for differentiating other glioma sub-groups: (i) IDH-mutant, 1p/19q^{ret} from IDH-mutant, 1p/19q^{codel} and (ii) IDH-mutant, 1p/19q^{ret} with AB/FS mismatch from IDH-mutant, 1p/19q^{ret} without AB/FS mismatch.

In our data, the amines range had at times a higher sensitivity than the amides range to distinguish between tumour types. Several groups have investigated the contributions to the CEST signal at 2ppm showing that the major contributions, at pH=7 and at a temperature of 37°C, come from: creatine (Cr), glutamate (Glu, roughly 40% of Cr signal), phosphocreatine (PCr), ATP (both approximately 20% of Cr signal), glucose (Glc, roughly 10% of Cr signal), and proteins [14], with various weightings of these different pools depending on the CEST saturation scheme and other MRI acquisition parameters. Some have suggested that at this pH and temperature, glutamine (Gln) does not contribute to the CEST signal at 2ppm [14], while others have found contribution from Gln, especially in tumours with a more acidic extracellular microenvironment [45]. It has also been suggested that also direct water saturation, semi-solid MT and water longitudinal relaxation time effects, which contribute to the signal non-linearly, are likely to contribute to the CEST signal at 2ppm [14]. It is possible that the presence of all these compounds at 2ppm increases the ability of the CEST signal at 2ppm to differentiate between tumour types. However, contributions from the NOE-mediated effect coming from the upfield resonances complicates the interpretations of our results and it may be the cause for the low sensitivity of the CEST amides signal for distinguishing between tumour types.

Limitations of the present study include the presence of the NOE-mediated effects in the MTRasym and DMTRasym spectra. The NOE-mediated contribution is reduced with increasing B_1 saturation power and saturation powers of 2mT had been shown in the past to null the NOE-mediated effect at 3.5ppm [40, 41]. Our normal appearing white matter MTR_{asym} signal nulls at 3ppm (Fig. 3A), therefore larger offsets

still have predominant NOE-mediated contributions. Our data acquisition was also limited to a single slice. Since the start of our study, 3D CEST sequences have become available at both 3T and 7T [46, 47] together with more complex analysis methods based on fitting multiple Lorentzian shapes to the data allowing the quantification of the different contributions from amides, amines, NOE, MT and water [32, 47]. We plan to introduce these acquisition and analysis strategies in our future studies, together with MRS and perfusion and diffusion measurements to further characterise gliomas both pre and post treatment.

Conclusions

The current study suggests that CEST-derived biomarkers for amines and amides, together with their ratio, which reflects in a composite manner tissue acidity and proteins/amino-acids abundance, can be used for histomolecular staging in a cohort of diagnostically challenging non- or low-enhancing gliomas. The data also suggests that the mismatch between CEST maps obtained with different models (asymmetry-based (AB) and fluid-suppressed (FS)) can be used to identify sub-groups in IDH-mutant, 1p/19q^{ret} gliomas that could potentially have prognostic and clinical relevance. CEST-derived biomarkers could therefore serve as risk stratification tools to inform oncologists of recurrence risk or of optimal treatment.

Abbreviations

1p/19q^{ret} = 1p/19q retained; 1p/19q^{codel} = 1p/19q codeleted; AB = Asymmetry Based; APT_w = Amines Proton Transfer weighted; AUC = Areas Under the receiver operating characteristics Curve; CEST = Chemical Exchange Saturation Transfer; DWI = Diffusion Weighted Imaging; GBM = glioblastoma; $DMTR_{asym}$ = changes in MTR_{asym}; FS = Fluid Suppressed; IDH = Isocitrate DeHydrogenase; MRS = Magnetic Resonance Spectroscopy; MTR_{asym} = Magnetization Transfer Ratio asymmetry; NAWM = Normal Appearing White Matter; NOE = Nuclear Overhauser Enhancement; ROE = Receiver Operating Characteristics.

The following do not need defining: AIDS; ANOVA; ATP; cDNA; CNS; CSF; CT; DNA; ECG; EEG; ELISA; EMG; GABA; HIV; MRI; PBS; PCR; PET; REM; RNA; mRNA; tRNA

Declarations

Funding

This project has received funding from the European Union's Horizon 2020 research and innovation programme under grant agreement No 667510 and the Department of Health's NIHR-funded Biomedical Research Centre at University College London. SB, XG and LM are supported by the National Institute of Health Research Biomedical Research Council, UCL Hospitals NHS Trust. EDV is supported by the Wellcome/EPSRC Centre for Medical Engineering [WT 203148/Z/16/Z].

Competing interests

The authors report no competing interests.

Availability of data and material

The authors confirm that the data supporting the findings of this study are available within the article, in its Supplementary material and/or from the corresponding author upon reasonable request.

Ethics approval

This prospective, on-going, investigator-initiated, single-centre, neuro-oncology imaging study received ethical and institutional review board approval (IRAS project ID: 210819; Research Ethics Committee reference: 16/LO/2081).

Consent to participate and for publication

All patients, prior to participation, provided written informed consent to participate and for publication.

References

1. Louis DN, Giannini C, Capper D, Paulus W, Figarella-Branger D, Lopes MB, et al. cIMPACT-NOW update 2: diagnostic clarifications for diffuse midline glioma, H3 K27M-mutant and diffuse astrocytoma/anaplastic astrocytoma, IDH-mutant. Acta Neuropathologica: Springer Verlag; 2018. p. 639-42.

2. Bisdas S, Shen H, Thust S, Katsaros V, Stranjalis G, Boskos C, et al. Texture analysis-and support vector machine-assisted diffusional kurtosis imaging may allow in vivo gliomas grading and IDH-mutation status prediction: A preliminary study. Scientific Reports: Nature Publishing Group; 2018.

3. Hempel JM, Brendle C, Bender B, Bier G, Kraus MS, Skardelly M, et al. Diffusion kurtosis imaging histogram parameter metrics predicting survival in integrated molecular subtypes of diffuse glioma: An observational cohort study. European Journal of Radiology: Elsevier; 2019. p. 144-52.

4. Kim M, Jung SY, Park JE, Jo Y, Park SY, Nam SJ, et al. Diffusion- and perfusion-weighted MRI radiomics model may predict isocitrate dehydrogenase (IDH) mutation and tumor aggressiveness in diffuse lower grade glioma. European Radiology: European Radiology; 2020. p. 2142-51.

5. Qi C, Yang S, Meng L, Chen H, Li Z, Wang S, et al. Evaluation of cerebral glioma using 3T diffusion kurtosis tensor imaging and the relationship between diffusion kurtosis metrics and tumor cellularity. Journal of International Medical Research; 2017. p. 1347-58.

6. Thust SC, Hassanein S, Bisdas S, Rees JH, Hyare H, Maynard JA, et al. Apparent diffusion coefficient for molecular subtyping of non-gadolinium-enhancing WHO grade II/III glioma: volumetric segmentation versus two-dimensional region of interest analysis. European Radiology: European Radiology; 2018. p. 3779-88.

7. Alsaedi A, Doniselli F, Jäger HR, Panovska-Griffiths J, Rojas-Garcia A, Golay X, et al. The value of arterial spin labelling in adults glioma grading: systematic review and meta-analysis. Oncotarget; 2019. p. 1589-601.

8. Brendle C, Hempel JM, Schittenhelm J, Skardelly M, Tabatabai G, Bender B, et al. Glioma Grading and Determination of IDH Mutation Status and ATRX loss by DCE and ASL Perfusion. Clinical Neuroradiology; 2018. p. 421-8.

9. Zhang J, Liu H, Tong H, Wang S, Yang Y, Liu G, et al. Clinical applications of contrast-enhanced perfusion MRI techniques in gliomas: Recent advances and current challenges. Contrast Media and Molecular Imaging: Hindawi; 2017.

10. Zikou A, Sioka C, Alexiou GA, Fotopoulos A, Voulgaris S, Argyropoulou MI. Radiation necrosis, pseudoprogression, pseudoresponse, and tumor recurrence: Imaging challenges for the evaluation of treated gliomas. Contrast Media and Molecular Imaging: Hindawi; 2018.

11. Suh CH, Kim HS, Jung SC, Choi CG, Kim SJ. 2-Hydroxyglutarate MR spectroscopy for prediction of isocitrate dehydrogenase mutant glioma: A systemic review and meta-analysis using individual patient data. Neuro-Oncology; 2018. p. 1573-83.

12. Usinskiene J, Ulyte A, Bjørnerud A, Venius J, Katsaros VK, Rynkeviciene R, et al. Optimal differentiation of high- and low-grade glioma and metastasis: a meta-analysis of perfusion, diffusion, and spectroscopy metrics. Neuroradiology; 2016. p. 339-50.

13. Van Zijl PCM, Yadav NN. Chemical exchange saturation transfer (CEST): What is in a name and what isn't? Magnetic Resonance in Medicine: John Wiley and Sons Inc; 2011. p. 927-48.

14. Zu Z, Louie EA, Lin EC, Jiang X, Does MD, Gore JC, et al. Chemical exchange rotation transfer imaging of intermediate-exchanging amines at 2 ppm. NMR in Biomedicine: John Wiley and Sons Ltd; 2017.

15. Su C, Liu C, Zhao L, Jiang J, Zhang J, Li S, et al. Amide proton transfer imaging allows detection of glioma grades and tumor proliferation: Comparison with Ki-67 expression and proton MR spectroscopy imaging. American Journal of Neuroradiology: American Society of Neuroradiology; 2017. p. 1702-9.

16. Togao O, Yoshiura T, Keupp J, Hiwatashi A, Yamashita K, Kikuchi K, et al. Amide proton transfer imaging of adult diffuse gliomas: Correlation with histopathological grades. Neuro-Oncology; 2014. p. 441-8.

17. Zhang J, Zhu W, Tain R, Zhou XJ, Cai K. Improved Differentiation of Low-Grade and High-Grade Gliomas and Detection of Tumor Proliferation Using APT Contrast Fitted from Z-Spectrum. Molecular Imaging and Biology: Molecular Imaging and Biology; 2018. p. 623-31.

18. Choi YS, Ahn SS, Lee SK, Chang JH, Kang SG, Kim SH, et al. Amide proton transfer imaging to discriminate between low- and high-grade gliomas: added value to apparent diffusion coefficient and relative cerebral blood volume. European Radiology: Springer Verlag; 2017. p. 3181-9.

19. Sakata A, Fushimi Y, Okada T, Arakawa Y, Kunieda T, Minamiguchi S, et al. Diagnostic performance between contrast enhancement, proton MR spectroscopy, and amide proton transfer imaging in patients with brain tumors. Journal of Magnetic Resonance Imaging; 2017. p. 732-9.

20. Togao O, Hiwatashi A, Yamashita K, Kikuchi K, Keupp J, Yoshimoto K, et al. Grading diffuse gliomas without intense contrast enhancement by amide proton transfer MR imaging: comparisons with diffusion- and perfusion-weighted imaging. European Radiology: Springer Verlag; 2017. p. 578-88.

21. Wen Z, Hu S, Huang F, Wang X, Guo L, Quan X, et al. MR imaging of high-grade brain tumors using endogenous protein and peptide-based contrast. NeuroImage; 2010. p. 616-22.

22. Ma B, Blakeley JO, Hong X, Zhang H, Jiang S, Blair L, et al. Applying amide proton transfer-weighted MRI to distinguish pseudoprogression from true progression in malignant gliomas. Journal of Magnetic Resonance Imaging; 2016. p. 456-62.

23. Mehrabian H, Desmond KL, Soliman H, Sahgal A, Stanisz GJ. Differentiation between radiation necrosis and tumor progression using chemical exchange saturation transfer. Clinical Cancer Research: American Association for Cancer Research Inc.; 2017. p. 3667-75.

24. Jiang S, Zou T, Eberhart CG, Villalobos MAV, Heo HY, Zhang Y, et al. Predicting IDH mutation status in grade II gliomas using amide proton transfer-weighted (APTw) MRI. Magnetic Resonance in Medicine: John Wiley and Sons Inc; 2017. p. 1100-9.

25. Yao J, Chakhoyan A, Nathanson DA, Yong WH, Salamon N, Raymond C, et al. Metabolic characterization of human IDH mutant and wild type gliomas using simultaneous pH- and oxygen-sensitive molecular MRI. Neuro-Oncology: Oxford University Press; 2019. p. 1184-96.

26. Joo B, Han K, Ahn SS, Choi YS, Chang JH, Kang SG, et al. Amide proton transfer imaging might predict survival and IDH mutation status in high-grade glioma. European Radiology: Springer Verlag; 2019. p. 6643-52.

27. Paech D, Dreher C, Regnery S, Meissner JE, Goerke S, Windschuh J, et al. Relaxation-compensated amide proton transfer (APT) MRI signal intensity is associated with survival and progression in high-grade glioma patients. European Radiology: Springer Verlag; 2019. p. 4957-67.

28. Regnery S, Adeberg S, Dreher C, Oberhollenzer J, Meissner J-E, Goerke S, et al. Chemical exchange saturation transfer MRI serves as predictor of early progression in glioblastoma patients. Oncotarget; 2018. p. 28772-83.

29. Keupp J, Togau O. Magnetisation transfer ratio based metric for APTw or CESTw MRI suppressing signal from fluid compartmentd - initial application to glioblastoma assessment. Proceedings of the International Society of Magnetic Resonance in Medicine; 2018. p. 3156.

30. Jin T, Wang P, Zong X, Kim SG. Magnetic resonance imaging of the Amine-Proton EXchange (APEX) dependent contrast. NeuroImage; 2012. p. 1218-27.

31. McVicar N, Li AX, Gonçalves DF, Bellyou M, Meakin SO, Prado MAM, et al. Quantitative tissue pH measurement during cerebral ischemia using amine and amide concentration-independent detection (AACID) with MRI. Journal of Cerebral Blood Flow and Metabolism: Nature Publishing Group; 2014. p. 690-8.

32. Windschuh J, Zaiss M, Meissner JE, Paech D, Radbruch A, Ladd ME, et al. Correction of B1-inhomogeneities for relaxation-compensated CEST imaging at 7T. NMR in Biomedicine; 2015. p. 529-37.

33. Yushkevich PA, Gao Y, Gerig G. ITK-SNAP: An interactive tool for semi-automatic segmentation of multi-modality biomedical images. Proceedings of the Annual International Conference of the IEEE Engineering in Medicine and Biology Society, EMBS: IEEE; 2016. p. 3342-5.

34. Stancanello J, Terreno E, Delli Castelli D, Cabella C, Uggeri F, Aime S. Development and validation of a smoothing-splines-based correction method for improving the analysis of CEST-MR images. Contrast Media and Molecular Imaging; 2008. p. 136-49.

35. Zhou J, Lal B, Wilson DA, Laterra J, Van Zijl PCM. Amide Proton Transfer (APT) Contrast for Imaging of Brain Tumors. Magnetic Resonance in Medicine: John Wiley and Sons Inc.; 2003. p. 1120-6.

36. Terreno E, Stancanello J, Longo D, Delli Castelli D, Milone L, Sanders HMHF, et al. Methods for an improved detection of the MRI-CEST effect. Contrast Media and Molecular Imaging; 2009. p. 237-47.

37. Patel SH, Poisson LM, Brat DJ, Zhou Y, Cooper L, Snuderl M, et al. T2–FLAIR mismatch, an imaging biomarker for IDH and 1p/19q status in lower-grade gliomas: A TCGA/TCIA project. Clinical Cancer Research: American Association for Cancer Research Inc.; 2017. p. 6078-86.

38. Lasocki A, Gaillard F, Gorelik A, Gonzales M. MRI features can predict 1p/19q status in intracranial gliomas. American Journal of Neuroradiology: American Society of Neuroradiology; 2018. p. 687-92.

39. Jaunmuktane Z, Capper D, Jones DTW, Schrimpf D, Sill M, Dutt M, et al. Methylation array profiling of adult brain tumours: diagnostic outcomes in a large, single centre. Acta neuropathologica communications: Acta Neuropathologica Communications; 2019. p. 24.

40. Zhao X, Wen Z, Huang F, Lu S, Wang X, Hu S, et al. Saturation power dependence of amide proton transfer image contrasts in human brain tumors and strokes at 3 T. Magnetic Resonance in Medicine: John Wiley and Sons Inc; 2011. p. 1033-41.

41. Zhou J, Hong X, Zhao X, Gao JH, Yuan J. APT-weighted and NOE-weighted image contrasts in glioma with different RF saturation powers based on magnetization transfer ratio asymmetry analyses. Magnetic Resonance in Medicine: John Wiley and Sons Inc; 2013. p. 320-7.

42. Intlekofer AM, Wang B, Liu H, Shah H, Carmona-Fontaine C, Rustenburg AS, et al. L-2-Hydroxyglutarate production arises from noncanonical enzyme function at acidic pH. Nature Chemical Biology: Nature Publishing Group; 2017. p. 494-500.

43. Lohmann P, Werner JM, Shah NJ, Fink GR, Langen KJ, Galldiks N. Combined amino acid positron emission tomography and advanced magnetic resonance imaging in glioma patients. Cancers: MDPI AG; 2019.

44. da Silva NA, Lohmann P, Fairney J, Magill AW, Oros Peusquens AM, Choi CH, et al. Hybrid MR-PET of brain tumours using amino acid PET and chemical exchange saturation transfer MRI. European Journal of Nuclear Medicine and Molecular Imaging: Springer Berlin Heidelberg; 2018. p. 1031-40.

45. Harris RJ, Cloughesy TF, Liau LM, Prins RM, Antonios JP, Li D, et al. PH-weighted molecular imaging of gliomas using amine chemical exchange saturation transfer MRI. Neuro-Oncology: Oxford University Press; 2015. p. 1514-24.

46. Akbey S, Ehses P, Stirnberg R, Zaiss M, Stöcker T. Whole-brain snapshot CEST imaging at 7 T using 3D-EPI. Magnetic Resonance in Medicine; 2019. p. 1741-52.

47. Deshmane A, Zaiss M, Lindig T, Herz K, Schuppert M, Gandhi C, et al. 3D gradient echo snapshot CEST MRI with low power saturation for human studies at 3T. Magnetic Resonance in Medicine: John Wiley and Sons Inc; 2019. p. 2412-23.

Tables

Table 1 Pairwise comparison of glioma groups for which the CEST metrics identify statistically significant differences. For the "two glioma types", p-values were calculated with Mann-Whitney U test, whilst for three and four glioma types p-values were calculated with Kruskal Wallis test followed, when significant, by the Conover-Iman test to correct for multiple pairwise comparisons. AUC is the area under the ROC curve. Threshold values (cut points) for the various metrics are reported together with their sensitivity and specificity

Group Comparison	Metric	p-value	AUC	Cut Point	
				value	Sensitivity / Specificity
Two glioma types: IDH-wildtype and IDH-mutant					
IDH-wildtype vs IDH-mutant	AB_APT$_w$(*D*2)	0.025	0.74	0.89	0.56 / 1.00
	FS_APT$_w$(*D*2)	0.050	0.71	0.60	0.67 / 0.67
	AB_APT$_w$ratio	0.0020	0.84	1.57	0.78 / 0.78
	FS_APT$_w$ratio	0.0045	0.81	1.66	0.78 / 0.78
	AB−FS(*D*2)	0.036	0.73	0.081	0.61 / 0.78
Three glioma types: IDH-wildtype; IDH-mutant, 1p/19q^{ret} and IDH-mutant, 1p/19q^{codel}					
IDH-wildtype vs IDH-mutant, 1p/19q^{ret}	AB_APT$_w$(*D*2)	0.0020	0.86	0.89	0.77 / 1.00
	FS_APT$_w$(*D*2)	0.014	0.81	0.76	0.68 / 0.89
	AB_APT$_w$ratio	0.0067	0.85	1.57	0.78 / 0.82
	FS_APT$_w$ratio	0.021	0.81	1.59	0.89 / 0.73
	AB−FS(*D*3.5)	0.032	0.79	0.048	0.64 / 0.78
	AB−FS(*D*2)	0.0066	0.85	0.081	0.82 / 0.78
IDH-wildtype vs IDH-mutant, 1p/19q^{codel}	AB_APT$_w$ratio	0.018	0.79	1.52	0.78 / 0.69
	FS_APT$_w$ratio	0.022	0.79	1.66	0.78 / 0.77
IDH-mutant, 1p/19q^{ret} vs IDH-mutant, 1p/19q^{codel}	AB_APT$_w$(*D*3.5)	0.035	0.74	1.43	0.55 / 0.92
	FS_APT$_w$(*D*3.5)	0.035	0.74	1.06	0.59 / 0.85
	AB_APT$_w$(*D*2)	0.0027	0.80	0.88	0.77 / 0.77
	FS_APT$_w$(*D*2)	0.015	0.76	0.77	0.68 / 0.85
	AB−FS(*D*3.5)	0.048	0.72	0.029	0.68 / 0.77
	AB−FS(*D*2)	0.015	0.76	0.14	0.68 / 0.85

Four glioma types: IDH-wildtype; IDH-mutant, 1p/19q^{ret} with AB/FS mismatch; IDH-mutant, 1p/19q^{ret} without AB/FS mismatch and IDH-mutant, 1p/19q^{codel}					
IDH-wildtype vs IDH-mutant, 1p/19q^{ret} with AB/FS Mismatch	$AB\_APT_w(D2)$	0.0001	0.97	0.89	0.93 / 1.00
	$FS\_APT_w(D2)$	0.0039	0.90	0.76	0.80 / 0.89
	$AB\_APT_w ratio$	0.0025	0.91	1.39	0.89 / 0.80
	$FS\_APT_w ratio$	0.032	0.85	1.59	0.89 / 0.80
	AB−FS(*D*3.5)	0.0005	0.92	0.067	0.80 / 0.89
	AB−FS(*D*2)	<0.0001	1.00	0.15	1.00 / 1.00
	AB−FS_ratio	0.037	0.81	−0.10	0.67 / 1.00
IDH-wildtype vs IDH-mutant, 1p/19q^{codel}	$AB\_APT_w ratio$	0.035	0.79	1.53	0.78 / 0.69
IDH-mutant, 1p/19q^{ret}: with AB/FS Mismatch vs without AB/FS Mismatch	$AB\_APT_w(D2)$	0.016	0.79	0.82	0.93 / 0.57
IDH-mutant, 1p/19q^{ret} with AB/FS Mismatch vs IDH-mutant, 1p/19q^{codel}	AB_APT_w(*D*3.5)	0.014	0.81	1.42	0.67 / 0.92
	FS_APT_w(*D*3.5)	0.025	0.79	1.28	0.67 / 0.92
	$AB\_APT_w(D2)$	0.0002	0.90	0.88	0.93 / 0.77
	$FS\_APT_w(D2)$	0.0049	0.85	0.77	0.80 / 0.85
	AB−FS(*D*3.5)	0.0007	0.85	0.042	0.93 / 0.85
	AB−FS(*D*2)	<0.0001	0.90	0.14	1.00 / 0.85
	AB−FS_ratio	0.039	0.76	−0.16	0.77 / 0.67
*D*3.5 = [3-4ppm] = 1ppm frequency range centred on the amides frequency at 3.5ppm; D2 = [1.5-2.5ppm] = 1ppm frequency range centred on the amines frequency at 2ppm; AB_APT_w(*Dw*) classic CEST metric in the *Dw* range (*Dw* = *D*3.5 or *Dw* = *D*2) normalised to the normal appearing white matter; FS_APT_w(*Dw*) = fluid suppressed CEST metric in the *Dw* range (*Dw* = *D*3.5 or *Dw* = *D*2);. $AB\_APT_w ratio$ = AB_APT_w(*D*3.5)/AB_APT_w(*D*2); $FS\_APT_w ratio$ = FS_APT_w(*D*3.5)/FS_APT_w(*D*2); AB−FS = AB_APT_w − FS_APT_w					

Table 2 Median values and 25 to 75 percentile ranges for the asymmetry-based (AB_APT_w) and fluid suppressed (FS_APT_w) normalised CEST metrics, for the various glioma groups and sub-groups

Metric	IDH-wildtype median (25 - 75 %tiles)	IDH-mutant median (25 - 75 %tiles)	IDH-mutant, $1p/19q^{ret}$ median (25 - 75 %tiles)	IDH-mutant, $1p/19q^{codel}$ median (25 - 75 %tiles)	IDH-mutant, $1p/19q^{ret}$ with AB/FS mismatch median (25 - 75 %tiles)	IDH-mutant, $1p/19q^{ret}$ without AB/FS mismatch median (25 - 75 %tiles)
$AB\_APT_w(D3.5)$	1.13 (0.79 - 1.37)	1.04 (0.84 - 1.61)	1.48 (0.96 - 1.77)	0.99 (0.61 - 1.06)	1.67 (0.97 - 1.82)	1.02 (0.76 - 1.51)
$FS\_APT_w(D3.5)$	1.07 (0.79 - 1.32)	1.03 (0.80 - 1.48)	1.33 (0.90 - 1.65)	0.98 (0.61 - 1.03)	1.47 (0.94 - 1.68)	1.00 (0.76 - 1.48)
AB_APTw(D2)	0.59 (0.48 - 0.75)	0.95 (0.61 – 1.13)	1.06 (0.92 - 1.40)	0.64 (0.49 - 0.85)	1.19 (0.97 - 1.50)	0.72 (0.38 - 1.09)
$FS\_APT_w(D2)$	0.56 (0.48 - 0.75)	0.73 (0.54 - 0.99)	0.90 (0.63 - 1.10)	0.59 (0.46 - 0.64)	0.96 (0.78 - 1.21)	0.63 (0.38 - 1.03)
AB_APT_wratio	1.74 (1.59 - 2.08)	1.30 (1.07 – 1.53)	1.26 (1.10 - 1.52)	1.34 (1.03 - 1.62)	1.21 (1.00 - 1.39)	1.52 (1.19 - 1.87)
FS_APT_wratio	1.90 (1.68 - 2.08)	1.45 (1.22 – 1.63)	1.44 (1.29 - 1.62)	1.44 (1.04 - 1.65)	1.38 (1.14 - 1.58)	1.52 (1.31 - 1.98)
AB−FS(*D*3.5)	0.003 (0 - 0.048)	0.032 (0.01 - 0.12)	0.08 (0.02 - 0.14)	0.010 (0.000 - 0.028)	0.12 (0.08 - 0.20)	0.018 (0 - 0.022)
AB−FS(*D*2)	0.015 (0.005 - 0.078)	0.12 (0.06 - 0.23)	0.20 (0.09 - 0.24)	0.07 (0.00 - 0.11)	0.22 (0.19 - 0.38)	0.069 (0 - 0.086)
AB−FS_ratio	−0.05 (−0.18 - −0.04)	−0.14 (−0.22 - −0.07)	−0.15 (−0.24 - −0.12)	−0.11 (−0.16 - 0)	−0.19 (−0.26 - −0.14)	−0.08 (−0.13 - −0.01)

*D*3.5 = [3 - 4ppm] = 1ppm frequency range centred on the amides frequency at 3.5ppm; D2 = [1.5 - 2.5ppm] = 1ppm frequency range centred on the amines frequency at 2ppm; $AB\_APT_w(Dw)$ asymmetry-based CEST metric in the *Dw* range (*Dw* = *D*3.5 or *Dw* = *D*2) normalised to the normal appearing white matter; $FS\_APT_w(Dw)$ = fluid suppressed CEST metric in the *Dw* range (*Dw* = *D*3.5 or *Dw* = *D*2);. AB_APT_wratio = $AB\_APT_w(D3.5)/AB\_APT_w(D2)$; FS_APT_wratio = $FS\_APT_w(D3.5)/FS\_APT_w(D2)$; AB−FS = $AB\_APT_w - FS\_APT_w$

Table 3 Sign test estimates of the differences between AB and FS CEST models for all the investigated metrics: amide signal, amine signal, signal ratio for amides/amines

Group	Metric		
	AB−FS(*D*3.5) median (25 - 75%tile) p-value	AB−FS(*D*2) median (25 - 75%tile) p-value	AB−FS_ratio median (25 - 75%tile) p-value
NAWM	0.0 (0.0 - 0.0) 1.0	0.0 (0.0 - 6.2e-06) 0.21	-
IDH-wildtype	0.003 (0 - 0.048) 0.29	0.015 (0.005 - 0.078) 0.0078	−0.05 (−0.18 - −0.04) 0.0078
IDH-mutant	0.032 (0.01 - 0.12) <0.0001	0.12 (0.06 - 0.23) <0.0001	−0.14 (−0.22 - −0.07) <0.0001
IDH-mutant, 1p/19q^{ret}	0.08 (0.02 - 0.14) <0.0001	0.20 (0.09 - 0.24) <0.0001	−0.15 (−0.24 - −0.12) <0.0001
IDH-mutant, 1p/19q^{codel}	0.010 (0.0 - 0.028) 0.0063	0.07 (0.0 - 0.11) 0.0018	−0.11 (−0.16 - −0.01) 0.0001
IDH-mutant, 1p/19q^{ret} with AB/FS mismatch	0.11 (0.08 - 0.20) 0.0001	0.22 (0.19 - 0.38) 0.0001	−0.19 (−0.25 - −0.13) 0.0001
IDH-mutant, 1p/19q^{ret} without AB/FS mismatch	0.018 (0 - 0.022) 0.22	0.069 (0.001 - 0.086) 0.016	−0.081 (−0.13 - −0.01) 0.016

*D*3.5 = [3 - 4ppm] = 1ppm frequency range centred on the amides frequency at 3.5ppm; D2 = [1.5 - 2.5ppm] = 1ppm frequency range centred on the amines frequency at 2ppm; AB−FS = AB − FS models; ratio = amides/amine ratio; diff = amides−amines; sum = amides+amines. p-values in bold represent statistically significant values. Threshold for significance p = 0.05.

Figures

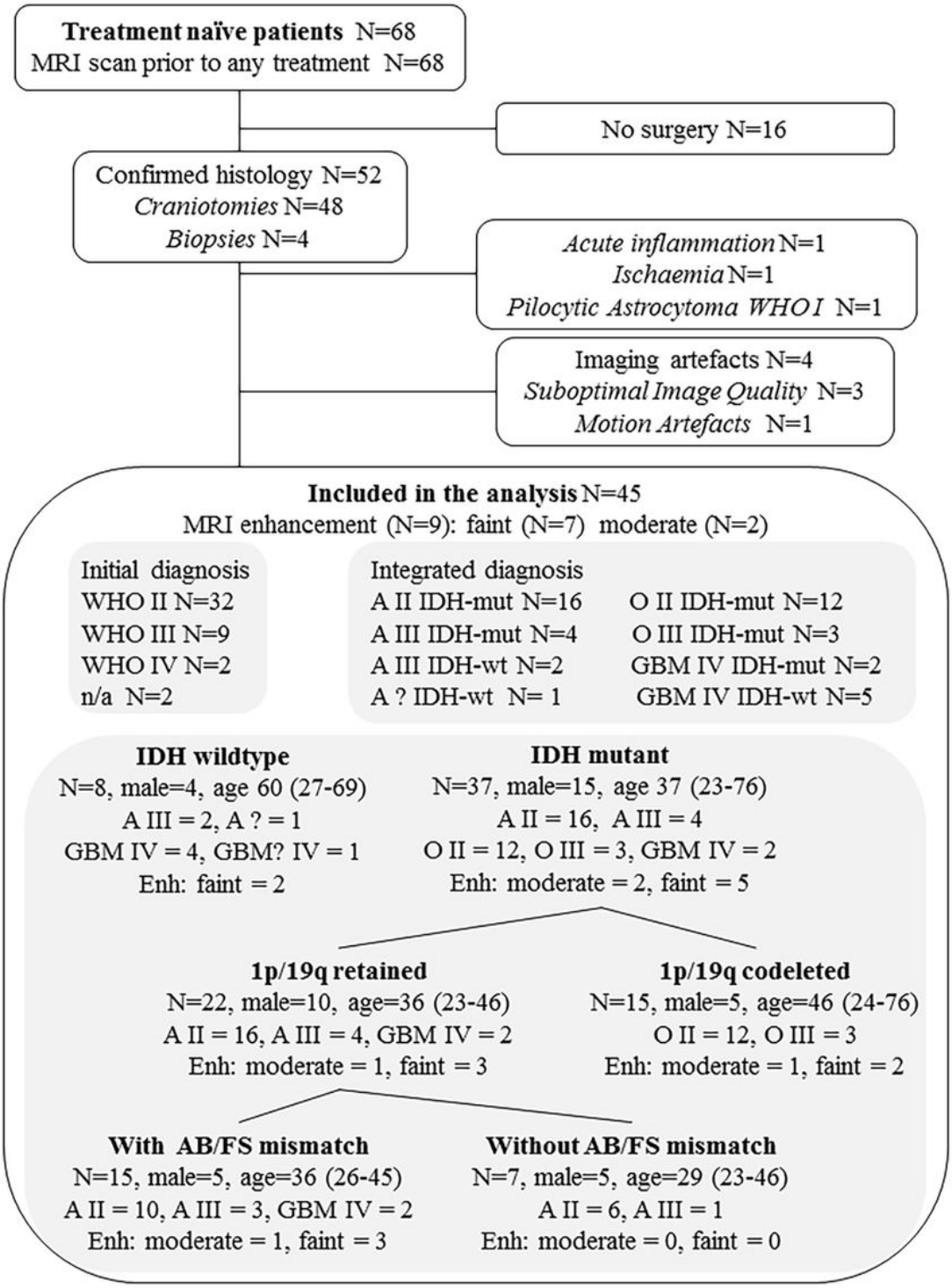

Figure 1

Patient recruitment and histology diagram. 45 histologically-proven glioma patients were included in this prospective study. All patients had an MRI scan prior to receiving any treatment. Surgery (craniotomies or biopsies) occurred a median (range) of 1.8 (0.1–30.7) months after MRI. A = astrocytoma, O = oligodendroglioma, GBM = glioblastoma; II, III, IV = WHO grades. Enh = subjects with post-gadolinium enhancement. Age is in years = median (range)

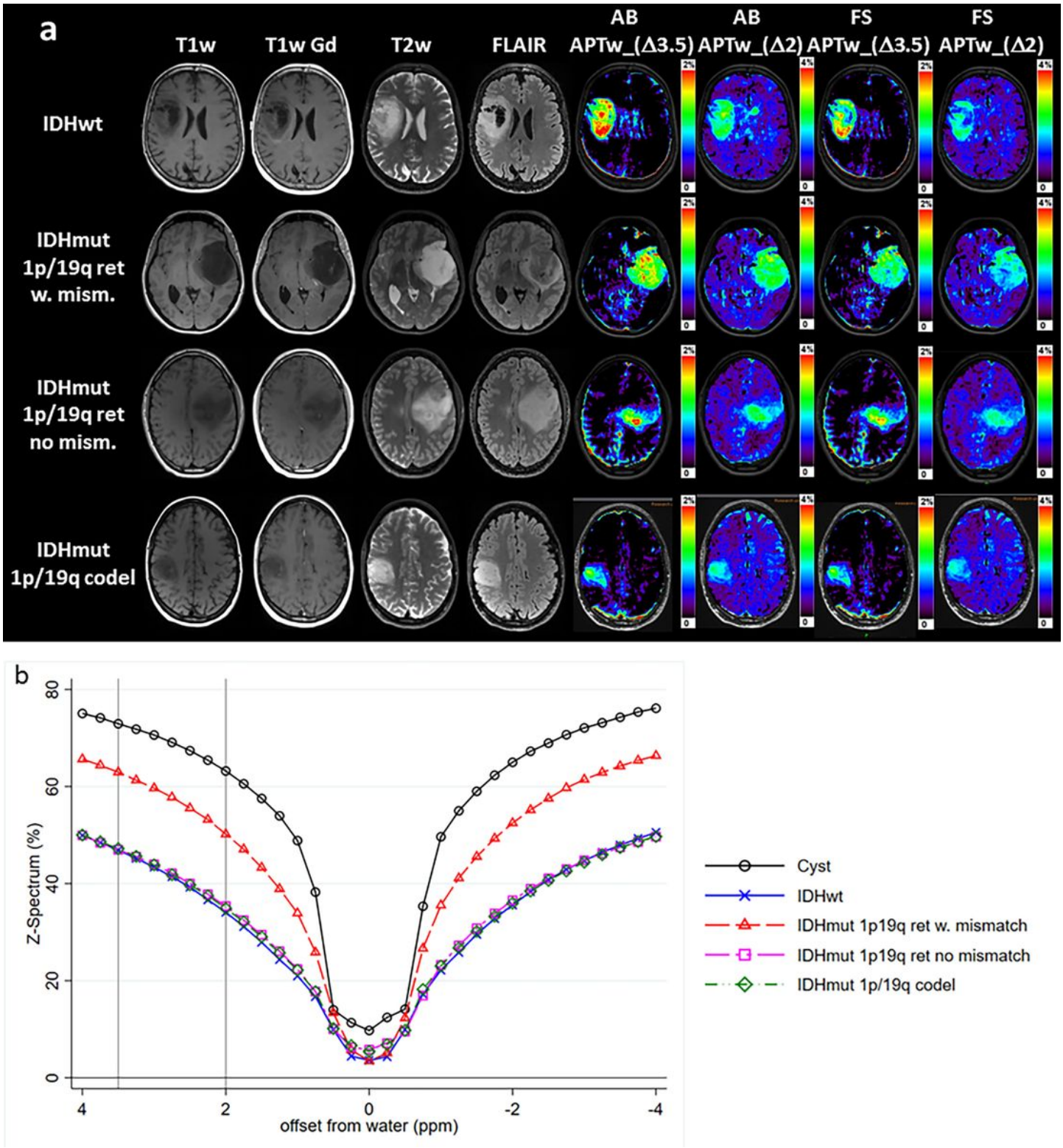

Figure 2

Representative examples of structural MRI, CEST maps and Z-spectra. (a) Representative structural MRI and CEST maps for IDH-wildtype, IDH-mutant, 1p/19qret with and without AB/FS mismatch, IDH-mutant, 1p/19qcodel. AB_APTw indicates the asymmetry-based metric while FS_APTw is the fluid-suppressed metric. 3.5 is the 1ppm offset range centred at the amides offset of 3.5ppm, while 2 is the 1ppm offset

range centred at the amines offset of 2ppm. (b) Representative Z-spectra of the cyst component and of the tumour core for the same tumour types

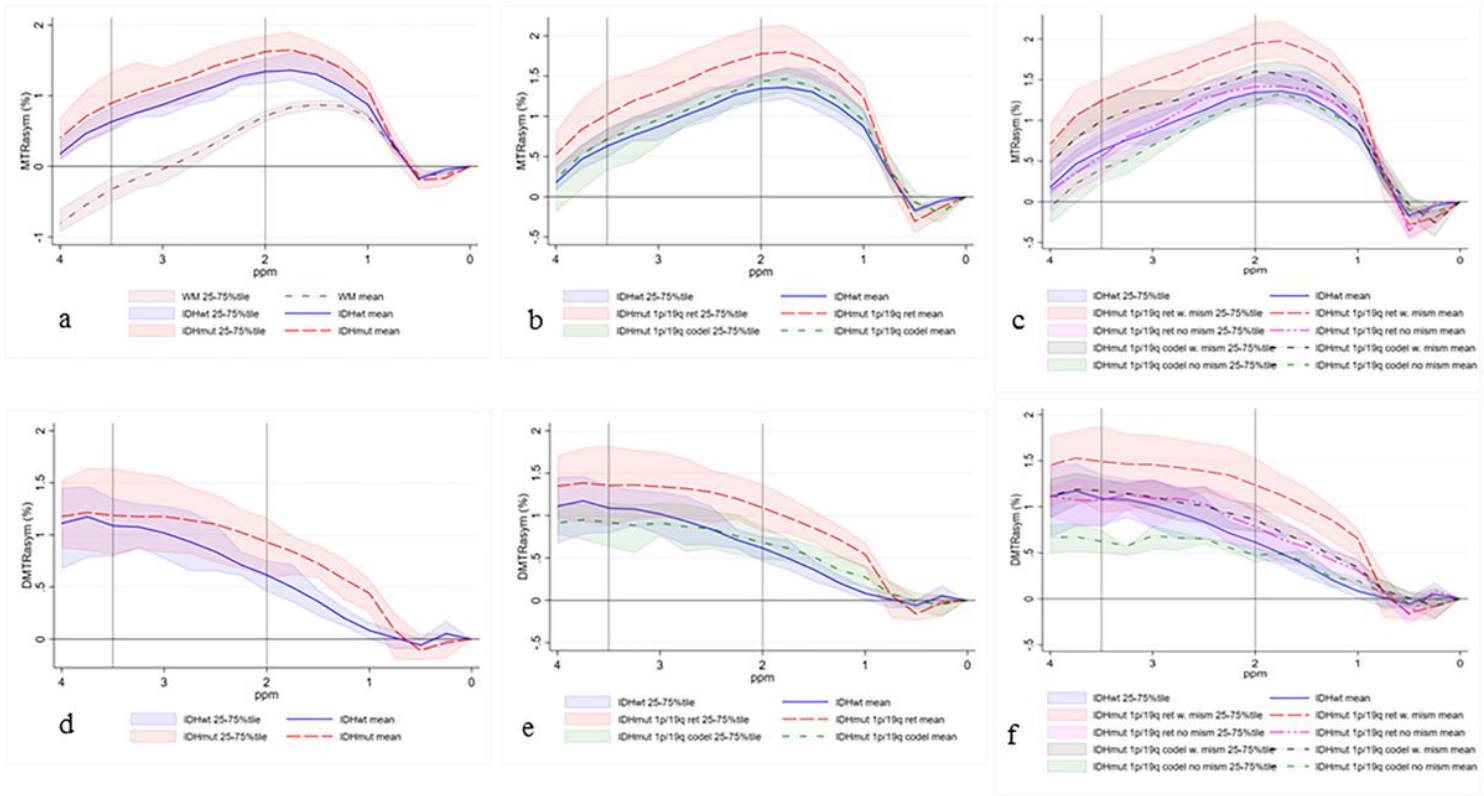

Figure 3

Comparison of the average MTRasym spectra (a, b, c) and average MTRasym spectra (d, e, f). The lines represent average values over tumour types. The shaded areas represent the range of variation between the 25th percentile and the 75th percentile. The vertical lines at 2ppm and 3.5ppm indicate, respectively, the center of the amines and of the amides regions. (a, d) IDH-wildtype vs IDH-mutant; (b, e) IDH-wildtype vs IDH-mutant, 1p/19qret vs IDH-mutant, 1p/19qcodel; (c, f) IDH-wildtype vs IDH-mutant, 1p/19qret with AB/FS mismatch vs IDH-mutant, 1p/19qret without AB/FS mismatch vs IDH-mutant, 1p/19qcodel. In (a), the average MTRasym spectrum of the contralateral normal appearing white matter (NAWM) is also shown, averaged over all patients

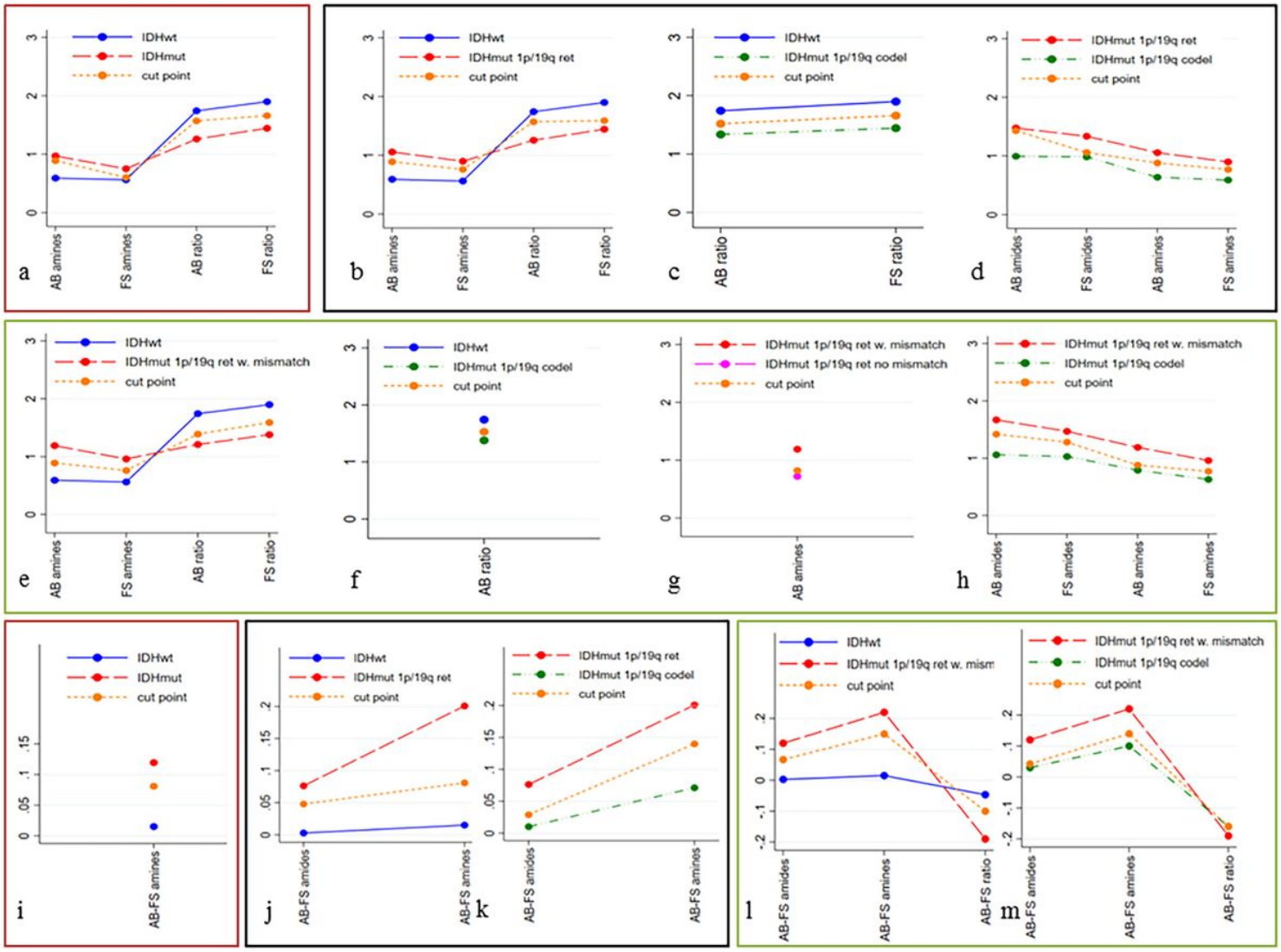

Figure 4

Pairwise comparison of groups with statistically significant differences in the represented metrics. The medians of the metrics are depicted, together with the cut points. (a - h) are the AB and AF metrics; (i - m) are the AB – FS metrics. (a) and (i): IDH-wildtype vs IDH-mutant. (b – d and j - k): three tumour types: IDH-wildtype, IDH-mutant, 1p/19qret, IDH-mutant, 1p/19qcodel. (e – h and l - m): Four tumour types: IDH-wildtype, IDH-mutant, 1p/19qret with (without) AB/FS mismatch, IDH-mutant, 1p/19qcodel

Supplementary Files

This is a list of supplementary files associated with this preprint. Click to download.

- 20210906ManciniCESTpapersupplementarymaterial.pdf